ChemElectroChem

Research Article
doi.org/10.1002/celc.202300639

Chemistry Europe
European Chemical Societies Publishing

www.chemelectrochem.org

Mott–Schottky Analysis of Historical and Archaeological Copper–based Objects

Antonio Doménech-Carbó,*[a] Marianne Mödlinger,[b] Laura Osete-Cortina,[c] and María Teresa Doménech-Carbó[d]

The application of Mott–Schottky (M–S) analysis of impedance data to sub–micro samples extracted from the corrosion patina of copper, bronze, and brass archaeological artifacts attached to graphite electrodes is described. The corresponding theoretical approach is developed to account for the contribution of the composition and structure of the corrosion patina and the effect of the bare graphite substrate. Experimental data in contact with 0.10 M Na_2SO_4 aqueous solution at pH 6.28 are consistent with the *p*-type semiconducting nature of the main copper corrosion products, cuprite, and tenorite. The values of the apparent flat band potential and the slope of the M–S plots allow archaeological samples to be grouped according to their M–S parameters (slopes and intercepts). Assuming equivalent conditions of corrosion, the resulting grouping is judged to be dependent on the composition, and/or method of manufacture, and/or age. Studied samples include Renaissance statues from the Hofkirche in Innsbruck and a variety of objects from museums and Archaeological Heritage Office (soprintendenza) in Austria (Bad Aussee, Johanneum Graz, and the Tyrolean State Museums), and Italy (Genoa and San Remo), dating from the Bronze Age to the 18th century. Complementary data are provided by voltammetry of immobilized particles.

Introduction

Obtaining information on the provenance, manufacturing technology and age of archaeological metal objects is important for archaeometric purposes.[1] This information is available from well–established microscopy, spectroscopy, and diffraction techniques.[2–5] However, in most cases, several factors limit their application to valuable, often unique, artifacts, in particular when the metallic core has to be accessed. As a result, there is increasing interest in the development of techniques that focus on the conservation and analysis of the corrosion patina of archaeological objects.[6–11]

To complement existing techniques, several patina–based electrochemical techniques have been proposed in the field of cultural heritage. These include in–situ electrochemical atomic force microscopy,[12] photoelectrochemical,[13] electrochemical impedance spectroscopy,[14,15] open–circuit potential measurements,[16,17] and voltammetry of immobilized particles (VIMP),[18–21] coupled to other techniques such as electron microscopy[18–21] and Raman spectroscopy.[22] Following its development by Scholz et al.,[23,24] the latter technique has been widely used in the study of cultural heritage due to the need for nanogram levels of sample.[25,26] VIMP sampling on copper/bronze objects allows the transfer of a series of micro–sheets from the patina adhering to the surface of graphite electrodes.[27,28] Application of multiple–scan procedures has been recently applied to obtain archaeometric information on copper/bronze artifacts.[27–29]

Here, we report a study of the application of a novel technique, Mott–Schottky (M–S) plots, derived from impedance measurements, to the study of archaeological metal patinas. This method exploits the semiconducting nature of the most common copper corrosion products (and eventually other patina components such as Sn and Zn oxides), cuprite (Cu_2O) and tenorite (CuO), both of which are *p*-type semiconductors with direct band gaps of 2.2 and 1.4 eV, respectively.[30,31]

The study is ultimately aimed to face a frequent problem in the historical and archaeologic domain: the grouping/screening of samples provided from insufficiently defined historical and archaeological contexts according to their composition and/or other factors such as provenance, manufacturing procedure, age and/or corrosion history. The basic idea is that, under equivalent ageing conditions, the differences in the composition and/or textural properties (compactness, crystallinity, porosity, …) of the patina reflect the differences in original manufacturing, composition, etc. We hypothesize that such

[a] Prof. Dr. A. Doménech-Carbó
Department of analytical chemistry
Dr. Moliner, 50, 46100 Burjassot (València) Spain
E-mail: Antonio.domenech@uv.es

[b] Dr. M. Mödlinger
Institut für Archaölogien
Universität Innsbruck
Langer Weg 11, 6020 Innsbruck, Austria

[c] Dr. L. Osete-Cortina
Institut für Archaölogien
Universität Innsbruck
Langer Weg 11, 6020 Innsbruck, Austria

[d] Prof. Dr. M. T. Doménech-Carbó
Institut de Restauració del Patrimoni
Universitat de València
Universitat Politècnica de València
Camí de Vera, 14, 46022 València, Spain

differences will be reflected in the semiconducting properties of the patina and, consequently, in the values of the M–S parameters. Accordingly, the values of these parameters should allow the grouping of homogeneous sets of samples.

The application of this technique for archaeometric purposes is discussed based on its application to many samples from Austrian museums (Bad Aussee, Joanneum Graz, Tyrolean State Museums (Hall deposit and Renaissance statues in the Hofkirche in Innsbruck)) and Italian museums and Archaeological Heritage Office (soprintendenza) (Genoa and San Remo). Most of these objects have previously been studied using conventional techniques.[32–36] The M–S data are complemented by electrochemical impedance spectroscopy (EIS) and VIMP measurements carried out on the same set of samples.

Results and discussion

Preliminary Impedance Measurements

The classical electrochemical approach to the study of semiconducting materials is based on the determination of the space charge capacity of films of the materials put in contact with aqueous electrolytes. As described in the following section, under certain conditions,[37] the Mott–Schottky equation applies to experimental electrochemical impedance data leading to the characterization of semiconducting materials. Concerning the potential application of this technique to the study of samples from metal patinas adhered to graphite electrodes, it is convenient to explore previously the suitability of impedance measurements for testing the semiconducting behavior of bare graphite and patinated metals.

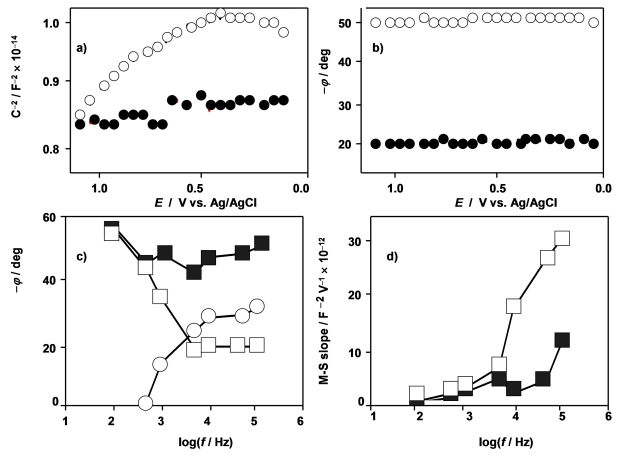

Figure 1. Impedance measurements on a bare graphite electrode (solid figures) and the same after sampling on a eurocent coin (empty figures). Electrolyte 0.10 M Na_2SO_4 (pH 6.28). a) Mott–Schottky plots at a frequency of 10^4 Hz; b) variation of the (minus) phase angle with the applied potential at a frequency of 10^4 Hz; c) variation of the averaged (minus) phase angle with the frequency (circles: the difference between eurocent-modified and unmodified electrode); d) variation of the apparent M–S slope with the frequency in the 0.5 to 1.1 V potential range.

Figure 1a shows the M–S plots obtained from impedance measurements carried out on a bare graphite electrode and the same after sampling a eurocent coin in contact with 0.10 M Na_2SO_4 aqueous solution at pH 6.28 and a frequency of 10^4 Hz. The capacitance values of the bare graphite show a slight variation in the range of potentials between 0.0 and 1.1 V vs. Ag/AgCl. In contrast, electrodes modified with samples extracted from the patina of Eurocent coins show a significant variation of capacitance with applied potential. In turn, the (minus)phase angle recorded at the same frequency for the sample-modified electrode remains essentially independent of the applied potential and differs significantly from the phase angle recorded for the bare graphite (Figure 1b). Repeated experiments give consistent results as shown in Figure S.1 of Supplementary Information. This results in $1/C^2$ vs. E plots that appear to be composed of two linear branches with similar negative slopes. These negative slopes are consistent with the *p*-type nature of the semiconducting components (cuprite and tenorite) of the corrosion patina.

The potential range used in impedance measurements was far from the potentials where the reduction of cuprite and tenorite oocur.

$$Cu_2O\ (solid) + 2H^+\ (aq) + 2e^- \rightarrow 2Cu\ (solid) + H_2O \quad (1)$$

$$CuO\ (solid) + 2H^+\ (aq) + 2e^- \rightarrow Cu\ (solid) + H_2O \quad (2)$$

These processes yield signals at −0.1 and −0.4 V.[26-29] However, this second signal is superimposed by some background current associated with the reduction of dissolved oxygen. When the potential scan is subsequently reversed, an anodic peak, often with peak splitting, is recorded at ca. 0.0 V.[26-29] This peak corresponds to the oxidative dissolution of the previously formed copper metal deposit to Cu^{2+} (aq) ions in the solution phase. In general, tin-localized voltammetric signals were absent, a result of the well–known destannification phenomenon[6–10]

Repeated impedance measurements in the same range of potentials at frequencies between 10^5 and 10^2 Hz revealed qualitatively similar characteristics. The variation of the averaged (minus) phase angle and the apparent M–S slope with the frequency are shown in Figures 1c and 1d, respectively. It can be seen that both parameters coincide for unmodified and sample–modified graphite electrodes at frequencies below 500 Hz. The difference in impedance parameters between unmodified and sample–modified electrodes increases rapidly at higher frequencies and tends to stabilize at frequencies between 10^4 and 10^5 Hz. Accordingly, these frequencies can be considered as indicative of obtaining information on the corrosion patina of archaeological samples adhered to graphite electrodes under our experimental conditions.

To model impedance measurements, it must be taken into account that the studied sample–modified working electrodes consist of a series of micrometer–sized laminations[27–29] deposited on a graphite base. For modeling purposes, EIS experiments were carried out at the OCP. Figure 2 shows the Nyquist

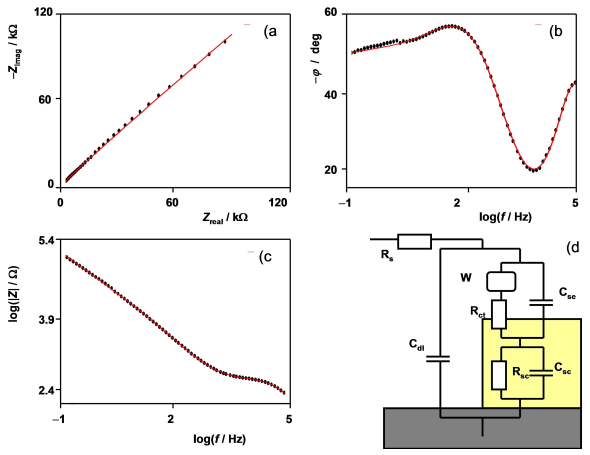

Figure 2. Impedance spectrum recorded at the OCP for a eurocent–modified graphite electrode in contact with 0.10 M Na_2SO_4 (pH 6.28). a) Nyquist plot of (minus)Z_{imag} vs. Z_{real}; b) Bode plot of (minus)phase angle vs. log*f*; c) Bode plot of log|*Z*| vs. log*f*; d) Equivalent circuit (see text). Experimental data points (circles) are superimposed to the theoretical spectrum (continuous line) taking $R_s = 87\ \Omega$, $C_{dl} = 0.014\ \mu F$, $R_{sc} = 342\ \Omega$, $C_{sc} = 1.0\times10^{-6}\ \mu F$, $R_{ct} = 12.9\ k\Omega$, $Q_{se} = 7.4\ \mu\Omega\,s^{-n}$ ($n = 0.78$), and $W = 0.072\ \mu\Omega\,s^{-1/2}$.

plot of the (minus)imaginary component of the total impedance (Z_{imag}) vs. the real component of the same quantity (Z_{real}) corresponding to the impedance spectrum recorded at the OCP for a eurocent–modified graphite electrode in contact with 0.10 M Na_2SO_4 solution at pH 6.28.

The experimental data points in Figures 2a–c can be satisfactorily fitted to the equivalent circuit shown in Figure 2d. Here, R_s represents the solution resistance and C_{dl} represents the double–layer capacitance associated with the interface between the electrolyte and the exposed graphite surface. The effect of the semiconducting sheets adhering to the graphite surface can be modeled by two parallel units of resistance plus capacitance. One corresponds to the double–layer capacitance (C_{se}) and charge transfer resistance (R_{ct}) across the semiconductor/electrolyte interface. The second corresponds to the capacitance (C_{sc}) and its associated resistance (R_{sc}) of the semiconducting patina. The best fit of the data was obtained by replacing the capacitor C_{se} by a constant phase element (Q_{se}) and adding the Warburg impedance (W) in series with R_{ct}. This situation is parallel to that described in the impedance analysis of microparticulate deposits and porous electrodes.[38]

Theoretical background

General aspects

As previously advanced, the type and density of charge carriers and the flat band potential of semiconducting materials can be determined from impedance data based on the Mott–Schottky equation:[37]

$$\frac{1}{C_{SC}^2} = \pm\frac{2}{N_D\varepsilon S^2 e}\left(E - E_{FB} - \frac{k_B T}{e}\right) \quad (1)$$

This equation predicts a linear variation of the inverse of the square of the space charge capacitance C_{SC} (F) with the applied potential, *E*. In this equation *e* is the electron charge, E_{FB} is the flat band potential, *S* is the electrode area (cm^2), and k_B is the Boltzmann constant. N_D is the density of charge carriers (cm^{-3}), corresponding to the electron donor concentration for an *n*-type semiconductor or the hole acceptor concentration for a *p*-type semiconductor. ε (F cm^{-1}) is the permittivity of the material equal to the product of the vacuum permittivity, ε_o, ($= 8.854\times10^{-14}$ F cm^{-1}) and the relative permittivity (the 'dielectric constant') of the material, ε'.

The $1/C_{SC}^2$ vs. *E* plot can be used for identifying the type of semiconductor: the slope is positive for *n*-type and negative for *p*-type, and for estimating the value of the flat band potential and the carrier density in the material. In practice, M–S plots are obtained from impedance measurements on solid films in contact with aqueous electrolytes using potential ranges where no faradaic processes occur. Usually, two simplifying hypotheses can be applied:

a) Strictly speaking, there are two capacitances to consider, that of the space charge region of the semiconducting material and that of the double layer at the material/electrolyte interface. As these capacitances are in series, the inverse of the total capacitance is the sum of their reciprocals. Since the space charge capacitance is much smaller than the double layer capacitance (typically 2–3 orders of magnitude), the contribution of the double layer capacitance to the total capacitance is negligible. Therefore, the capacitance value calculated from this model is assumed to be the value of the space charge capacitance.
b) The capacitance element is connected in series with a resistor so that the instrumentation provides the imaginary part of the total impedance. To minimize the contribution of the resistance to the total impedance, it is convenient to make measurements at frequencies in the kHz range.

Figure 3a shows a scheme for the band diagram of cuprite and tenorite. It should be noted that the E_{FB} is approximately equal to the conduction and valence band edges for *n*-type and *p*-type conductors, respectively,[37] but can vary significantly depending on the material structure. For example, the E_{FB} for pure cuprite under similar experimental conditions to those used here was 0.55 V vs. RHE but becomes 1.13 V vs. RHE for Cu_2O–CuO heterojunctions.[31] In addition, we assume that band gap broadening due to quantum size effects[39–41] and those due to the variation of the donor/acceptor density with the applied potential[42] are negligible.

Continuous patinas

Let us assume that the electrode is formed by a homogeneous semiconducting band consisting of a mixture of cuprite and tenorite as schematized in Figure 3b. Ideally, the composition

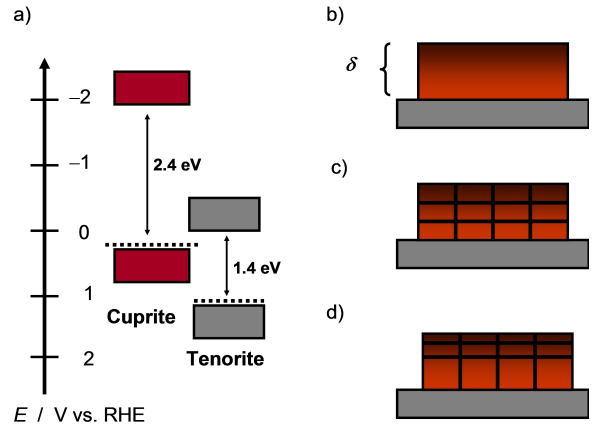

Figure 3. a) Energy band diagram for cuprite and tenorite based on data from.[32,33] The dotted lines mark the valence band edges, corresponding approximately to the respective flat band potentials. The double arrows correspond to the forbidden energy band. b–d) Schematic representations of the corrosion patina as a continuous layer (b) and as a set of cuboids of equal size (c) and different sizes (d) distributed in columns separated by intergranular material.

will be reflected in the value of the relative permittivity, ε′. In the simplest view, this would be intermediate between those reported for cuprite ($\varepsilon'_{CUP} = 16.2$) and tenorite ($\varepsilon'_{TEN} = 18.1$),[43]

$$\varepsilon' = \alpha_{TEN}\varepsilon'_{TEN} + (1-\alpha_{TEN})\varepsilon'_{CUP} \quad (2)$$

where α_{TEN} represents the molar fraction of tenorite in the corrosion layer assumed to be homogeneous. Since $\varepsilon'_{TEN} > \varepsilon'_{CUP}$, one would expect the slope of the MS plot to be greater in the inner (tenorite–poor) region of the patina than in the outer (tenorite–rich) region. However, given the similarity between the values of ε'_{CUP}, and ε'_{TEN}, no significant changes in the capacitance (and hence in the MS slope) associated with the compositional change in the corrosion patina can be expected. This 'macroscopic' view ignores the fact that cuprite and tenorite are formed as separate phases and a contact potential difference is necessarily established between them.

Granular patinas

The above 'homogeneous' view also ignores that the patina is formed by the aggregation of grains (microcrystals) of the mineral components. Among other possibilities, studies of tenorite enrichment on multiple entropy–stabilized oxides[44] reveal that a secondary phase of tenorite has formed occupying intergranular spaces between the cuprite grains. The effect is to create a conductive percolation path which increases charge transport and the effective dielectric constant.

The simplest way to model this system is to represent the corrosion patina as a series of homogeneous cuboid grains of equal size distributed in columns separated by intergranular deposits as schematized in Figure 3c. The total number of cuboids, *N*, can be estimated as the product of the number of layers, δ/a, and the number of cuboids per layer, S/a^2, i.e.,

$$N = \left(\frac{\delta}{a}\right)\left(\frac{S}{a^2}\right) = \frac{\delta S}{a^3} \quad (3)$$

The capacity of this system, relative to the charge separation between the cuboid–cuboid interface can be estimated as the result of the parallel combination of S/a^2 columns each one containing the series association of δ/a cuboids. In each column, we can consider the capacitance associated with each cuboid, the capacitance associated with the intergranular component (possibly tenorite occupies intergranular locations), and the capacitance associated with the contact grain/intergranular material. The capacitance associated with each cuboid is,

$$C_{cub} = \varepsilon_{cub}\frac{a^2}{a} = a\varepsilon_{cub} \quad (4)$$

where εc_{ub} represents the dielectric permittivity of the cuboids. In turn, the capacity of the intergranular regions interposed between the cuboids is,

$$C_{int1} = \varepsilon_{int}\frac{a^2}{\lambda} \quad (5)$$

where ε_{int} is the dielectric permittivity of the intergranular material assumed to be homogeneous and λ the intergranular distance. In addition, we can consider a capacitance term associated with the contact between the cuboid and intergranular regions, C_X. In a column, all these capacitors are in series so that the total capacitance of one column is:

$$\frac{1}{C_{column}} = \frac{1}{C_{cub}} + \frac{1}{C_{int}} + \frac{1}{C_X} \quad (6)$$

Assuming that a second portion of the intergranular material forms columns interposed between the columns of cuboids, the capacitance of each column of intergranular material is,

$$C_{lat2} = \varepsilon_{int}\frac{\lambda a}{\delta} \quad (7)$$

Since the columns of cuboids and intergranular material are located in parallel between them, the total capacitance is (see Figure 3c),

$$C = \frac{S}{a^2}(C_{column} + 4C_{lat2}) \quad (8)$$

Combining the above equations, the total capacity of the patina can be expressed as,

$$C = \frac{S}{\delta}\left[\frac{\varepsilon_{cub}\varepsilon_{int}C_X a}{\varepsilon_{int}C_X a + \varepsilon_{cub}C_X\lambda + \varepsilon_{cub}\varepsilon_{int}a^2} + 4\varepsilon_{int}\frac{\lambda}{a}\right] = \varepsilon_{eff}\frac{S}{\delta} \quad (9)$$

Here, ε_{eff} is an effective dielectric permittivity function of the cuboid size a, the intergranular distance,λ, the dielectric permittivities of the respective materials. In principle, one can assume that $\lambda \ll a$ and $\varepsilon_{int} \approx \varepsilon_{cub}$, so that Eq. (9) becomes,

$$C \approx \frac{S}{\delta}\left[\frac{\varepsilon_{cub}\varepsilon_{int}C_X}{\varepsilon_{int}C_X + \varepsilon_{cub}\varepsilon_{int}a}\right] \tag{10}$$

If the term C_X does not apply the capacitance is,

$$C \approx \frac{S}{\delta}\left[\frac{\varepsilon_{cub}\varepsilon_{int}}{\varepsilon_{int} + \varepsilon_{cub}(\lambda/a)} + \varepsilon_{int}\left(\frac{\lambda}{a}\right)^2\right] \tag{11}$$

This means that neglecting possible contact effects, the total capacitance depends on the λ/a ratio. As previously noted, under our experimental conditions, $\lambda \ll a$ and $\varepsilon_{int} \approx \varepsilon_{cub}$, so that one can approximate to,

$$C \approx \frac{S}{\delta}\left[\frac{\varepsilon_{cub}}{1 + (\lambda/a)}\right] \tag{12}$$

This means that the total capacity will decrease as the λ/a ratio decreases. The above equation reduces to that for a homogeneous patina ($C = \varepsilon_{cub}S/\delta$) when $\lambda = 0$.

Discontinuous Deposits

The above treatment applies to continuous films of the semiconducting material forming the working electrode. Our systems, however, consist of a series of micrometer–sized laminations[27–29] deposited on a graphite base electrode forming a discontinuous deposit. This can be described by the equivalent circuit in Figure 2.

According to the simplified scheme in Figure 4 (inset), the measured capacitance C results from the contribution of the parallel combination of the exposed graphite and the patina layers. The latter in turn results from the series combination of the space charge and the double layer capacitances. We can assume that the patina plates cover a small fraction of the graphite surface so that C_{graf} can be considered constant. However, the space charge capacity will depend on the size and number of patina sheets. Assuming that our sample-modified electrode contains K identical sheets extracted from the patina of the metal object, the measured capacitance, C, will be:

$$C = KC_{SC} + C_{graf} \tag{13}$$

where C_{SC} is the space charge capacitance of a single plate. According to the M–S model (Eq. (1)), this quantity varies with the applied potential as,

$$\frac{1}{C_{SC}^2} = \pm\frac{2}{N_D\varepsilon_{eff}e}\left(E - E_{FB} - \frac{k_BT}{e}\right) = \pm[A + B(E - E_{FB})] \tag{14}$$

Then, combining Eqs. (13) and (14)

$$\frac{1}{C^2} = \frac{A + B(E - E_{FB})}{K^2 + C_{graf}^2[A + B(E - E_{FB}] + 2KC_{graf}[A + B(E - E_{FB})]^{1/2}} \tag{15}$$

At potentials where $C_{graf} \ll [A + B(E\text{-}E_{FB})]^{-1/2}$,

$$\frac{1}{C^2} \approx \frac{A + B(E - E_{FB})}{K^2} \tag{16}$$

Then, the $1/C^2$ vs. E plot will tend to a straight line with slope B/K^2 and intercept $(A - BE_{FB})/K^2$. The intercept/slope ratio will be $A/B - E_{FB}$, a K-independent quantity. At potentials where $E\text{-}E_{FB} \approx 0$, one can approximate,

$$\frac{1}{C^2} \approx \frac{A + B(E - E_{FB})}{K^2 + C_{graf}^2A + 2KC_{graf}A^{1/2}} \tag{17}$$

Now, the plots of $1/C^2$ vs. E will give straight lines of slope SL given by,

$$SL = \frac{B}{K^2 + C_{graf}^2A + 2KC_{graf}A^{1/2}} \tag{18}$$

and intercept OO,

$$OO = \frac{A - BE_{FB}}{K^2 + C_{graf}^2A + 2KC_{graf}A^{1/2}} \tag{19}$$

The ratio between these two quantities is independent on K, so that there will be a linear relationship between OO and SL:

$$OO = \left(\frac{A}{B} - E_{FB}\right)SL \tag{20}$$

It is worth noting that the contribution of the different capacitance elements depends on the frequency used in the

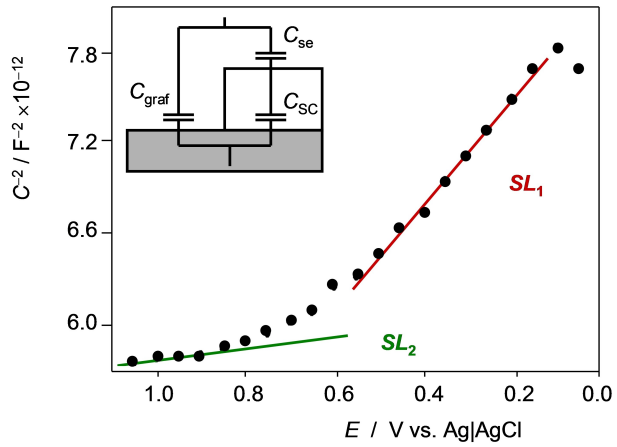

Figure 4. $1/C^2$ vs. E plot for Graz sample 2862 (axe, Buchkogel/Wildon 2480, 02480; Archäologiemuseum, cat. no. 312, dated back to late Urnfield Culture, 1200–900 BCE) in contact with 0.10 M Na_2SO_4 (pH 6.28). Frequency 1000 Hz. Experimental data points (black circles) and straight trend lines illustrate the corresponding M–S parameters. Inset: Simplified combination of capacitances.

impedance measurements. The data in section 3.1 shows that at low frequencies (approximately below 500 Hz) the C_{graf} term dominates over the KC_{SC} term in Eq. (13). This means that impedance measurements at low frequencies will become insensitive to the properties of the patina sheets. Accordingly, high–frequency impedance measurements should be used to group/discriminate archaeological metal samples.

For our purposes, there are several aspects to underline:

i) The net amount of patina adhering to the graphite surface will vary in each experiment. Therefore, the absolute values of *C* will vary in replicate experiments on the same patina. However, the *OO*/*SL* ratios will be the same.

ii) The values of the M–S parameters *A* and *B* in the preceding equations reflect the charge carrier density and the dielectric permittivity of the patina. Accordingly, they will depend on the composition and structure of the corrosion patina.

iii) The flat band potential reflects the bending in the band structure of the semiconductor and can also be considered as a patina characteristic. As judged from recent studies on Cu_2O–CuO heterostructures,[31] and cuprite–based patinas,[45–48] the E_{FB} is significantly influenced by the structural properties of the junctions. Accordingly, it is reasonable to expect that E_{FB} values will differ in corrosion patinas containing cuprite and tenorite with different degrees of compactness and crystallinity.

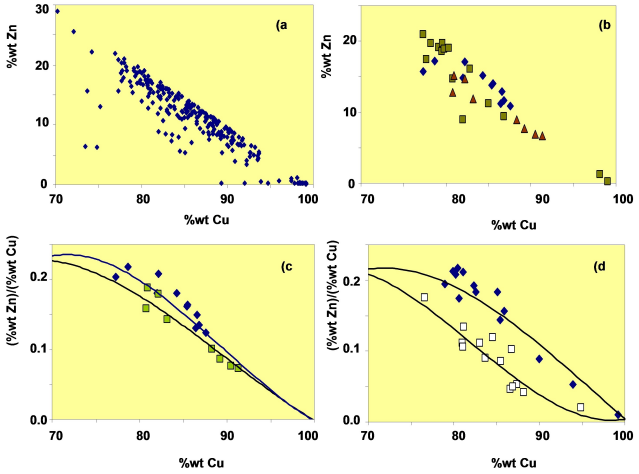

Figure 5. a) Values of the percentages of Cu and Zn from XRF data of Hofkirche in Innsbruck statues (sampling in 4–12 different regions of each statue) in this study. b) The same representation for statues HK01 (rhombs), HK10 (squares), and HK09 (triangles). c) Variation of the (% wt Zn)/(% wt Cu) ratio on the percentage of copper determined from XRF data measured in several points of Hofkirche in Innsbruck statues HK01 (rhombs), and HK10 (squares). D) The same representation for sample HK11 (rhombs) and the brass plaques (squares) at Hall deposit of the Tyrolean State Museums. Continuous lines correspond to polynomial functions of degree 3.

Historical and Archaeological Samples

In all cases, well–defined-M–S plots of C^{-2} v.s *E* were obtained. As a representative example, Figure 4 shows the M–S plot generated from the experimental impedance data for Graz sample 2862 (axe, Buchkogel/Wildon 2480, 02480; Archäologie-museum, cat. no. 312, dated back to the Late Bronze Age (1200–900 BCE) in contact with 0.10 M Na_2SO_4 (pH 6.28). In this figure, the experimental data points (black circles) are accompanied by the straight trend lines (1 and 2) at low and high potentials. To compare different samples we will use the slopes (SL_1, SL_2) and intercepts (OO_1, OO_2), defined according to the criteria in Figure 4) of these straight lines.

First, we compared the M–S parameters for a set of samples that can be considered as highly homogeneous, the 24 brass statues of the Hofkirche Innsbruck. This corresponds to a series of statues made in several workshops during the first half of the 16th century CE whose production is well known from the historical documentation.[49,50] The composition was studied by surface XRF[36] suggesting a relatively homogeneous composition. This is a common feature in historic and archaeological metal, whose elemental composition usually varies within narrow ranges.[51]

It is worth noting that surface XRF analyses cannot provide the composition of the metal core of the objects.[51,52] XRF analyses carried out in different regions of the same statue (4–12 data points were taken depending on the shape and size of the statue) revealed large variations in the Cu and Zn contents.[36] This is illustrated in Figure 5a where the entire set of composition data is summarized by plotting % wt Zn vs. % wt Cu.

Surface XRF data show large variations in the Cu and Zn contents in different regions of each statue. This is due to the fact that this technique provides an averaged composition of the outer region of the object more or less deep depending on the local X-ray penetration. Figure 5b compares the results for three statues showing the variation in the Cu and Zn contents.

In these circumstances, an estimate of the composition of the metallic core of the objects can be made by assuming that, due to the general phenomena of destannification and dezincation,[10] one can assume that the percentage of Zn (Sn in the case of bronze) will be depleted from the inner to the outer layers of the patina. Figure 5c illustrates a potential way of estimating the Zn/Cu ratio in the metal core from XRF data. Plotting the (% wt Zn)/(% wt Cu) ratio vs. the % wt Cu, the data points can be approximated to s-shaped curves that tend towards a maximum Zn to Cu ratio. The plateau in the above plot will correspond to the composition of the metallic core. Our data reveal a quite similar composition of the statues (17 ± 2 % wt Zn). As can be seen in Figure 5c, where data for statues HK 01 and HK 10 are superimposed, the only relevant difference between them corresponds to the profile of the curved path, not to the base metal composition.

Given the similarity in the composition of the metallic core and the similarity in the corrosion conditions, such differences can be attributed mainly to differences in the manufacturing procedure. The above data can be compared with those obtained for brass plaques from the deposit in Hall of the Tyrolean State Museums. Note that, in this case, due to the small size of the objects a unique XRF data point was obtained for each plaque. The resulting (% wt Zn)/(% wt Cu) vs. % wt Cu

plot (Figure 5d) can be approached to an s-shaped curve with the same plateau as the statues in the Innsbruck Hofkirche but a different dezincation profile (illustrated for statue HK11 in Figure 5d). This result suggests that the base metal was of the same composition for both sets of samples, but that the statues and the plaques differ in their respective manufacturing procedures and/or corrosion history.

To test whether these differences are reflected in the M–S response, the variation of the apparent flat band potential corresponding to the intercept of the first trend line, OO_1, on the slope of the same line, SL_1 was tested for the above samples. Figure 6 shows the data points recorded for the brass statues from Hofkirche in Innsbruck and the brass plaques from the Tyrolean State Museums fabricated between the 15th and 17th centuries CE. These samples can be grouped around two different almost linear tendency lines (except for sample HK10) separating the statues and the plaques. This denotes that, consistently with XRF data, M–S parameters are sensitive to differences in the manufacturing technique and/or corrosion history of the objects.

Restricting the M–S analysis to the Hofkirche in Innsbruck brass statues, the main group of samples corresponds to statues cast in the workshops of Godl, Sesselschreiber, P. Vischer the Younger, and G. Löffler (see also Figure S.2 of Supplementary Information). The 'anomalous' data point corresponds to sample HK10, just the unique sculpture cast by P. Löffler/Leiminger in 1509 (see Tables S.1 and S.2). Given the common metal base composition derived from the XRF data and the uniformity of the corrosion history (from historic information), the M–S data analysis suggests that the earlier workshops used quite similar casting techniques, different from those used in the Löffler/Leiminger workshop. The sensitivity of M–S data to subtle changes in the properties of the objects is in agreement with previous voltammetric studies on ancient coins allowing us to discriminate different series of coinages.[20–22] Voltammetric data were found to be entirely consistent with Raman spectroscopy for discriminating historic mints.[17,22]

The data recorded for a series of brass plaques in the Hall Museum dating from the 15th to 17th centuries CE (see Tables S.3 and S.4 in the Supplementary Information) are also shown in Figure 6. Interestingly, this data set falls within a potential trend curve with an exponent of 0.83. Given the similarity in composition and the relative similarity in age, the difference between the two data sets can be mainly attributed to differences in manufacturing and 'corrosion history'.

Figure 7 illustrates the influence of the frequency used in impedance measurements. It shows the OO_1 vs. SL_1 plots for archaeological bronze samples of Roman (1st–2nd century CE) and Bronze Age/Iron Age samples from the sopraintendenza of Genoa and bronze samples of Roman (1st–2nd century CE) and Bronze Age from the museo civico of San Remo recorded at frequencies of 10^4 and 10^2 Hz (see Tables S.7 and S.8). These are relatively homogeneous sets of samples. Samples GE02, GE05, GE10, GE11, GE12, GE24 come from different archaeological sites around the city of Albenga, all Roman age (1st–2nd century CE), and samples GE13-GE23 were recovered in the site of Sassello, assigned to the Bronze Age/Iron Age. In turn, SR02-SR08 samples correspond to Roman, objects from the sites of Promontorio dell'Arma, Castellaro di Monte Colma, and the Necropoli di San Lorenzo all in the close vicinity of San Remo, and dated to 1st–2nd century CE, whereas samples SR11a–SR11 h correspond to a unique Bronze Age bracelet from the site of Buco del Diavolo (Realdo).

It can be seen that experimental data points recorded at 10^2 Hz show a relatively large spread and no discrimination between Bronze Age and Roman Age samples. This is consistent, as previously discussed, with the predominance of the contribution to the total capacitance at low frequencies from the exposed graphite/electrolyte interface. In contrast, the impedance data at 10^4 Hz, grouped the experimental data

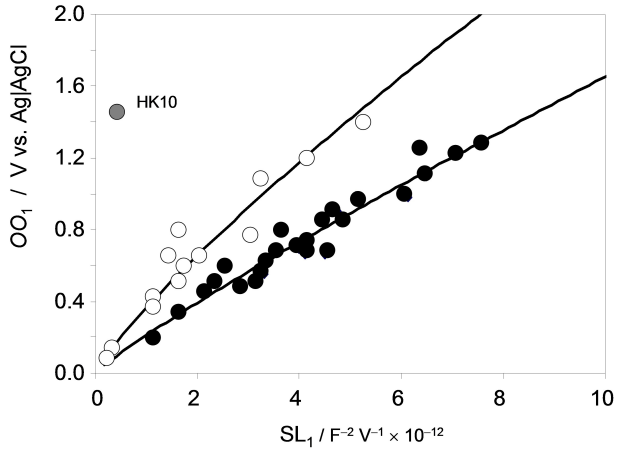

Figure 6. Variation of the OO_1 on SL_1 of the M–S representations corresponding to brass samples from the Renaissance statues from the Hofkirche in Innsbruck produced in the first half of the 16th century CE (solid circles) and plaques (circles) from the Tyrolean State Museums fabricated between the 15th and 17th century CE. The grey circle corresponds to sample HK10 (see text). The continuous lines correspond to the fitting of experimental data to potential functions. From impedance measurements such as depicted in Figure 4.

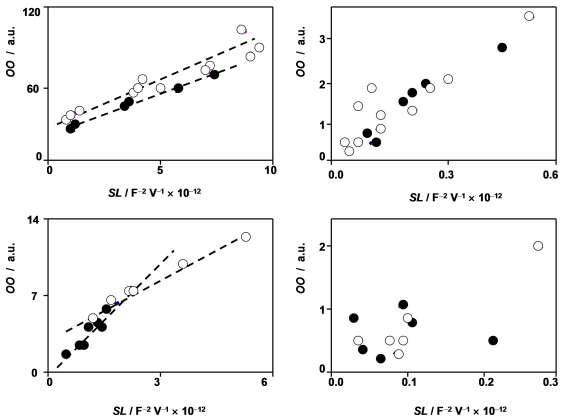

Figure 7. Plots of OO_1 vs. SL_1 for archaeological bronze samples, a,b) GE02, GE05, GE10, GE11, GE12, GE24 (Roman 1th-2th CE, solid circles) and GE13-GE23 (Bronze Age/Iron Age, circles) from the sopraintendenza of Genoa, and c,d) SR02-SR08 (Roman, 1th-2th CE, solid circles) and SR11a-SR11 h (Bronze Age, circles) from the museo civico of San Remo. Impedance measurements in conditions such as previous figures at a,c) 10^4 Hz, b,d) 10^2 Hz. The dotted lines represent the approximate fit of experimental points to straight lines.

points into well–defined trend lines, distinguishing between Bronze Age and Roman Age samples. In Figure 7, the approximate trends consistent with Eq. (20) are shown as dotted straight lines.

This sensitivity can also be seen when considering a series of samples of binary (Cu–Sn) bronze and almost pure copper from the Urnfield Culture (1200–900 BCE) from the Johanneum of Graz (see Supplementary Information, Tables S.5 and S.6). As can be seen in Figure 8, the corresponding E_{FB1}^{app} vs. SL_1 plot, the data points for both series of objects define potential trend curves whose respective exponents, 0.80 and 0.77, differ from the series in Figure 6.

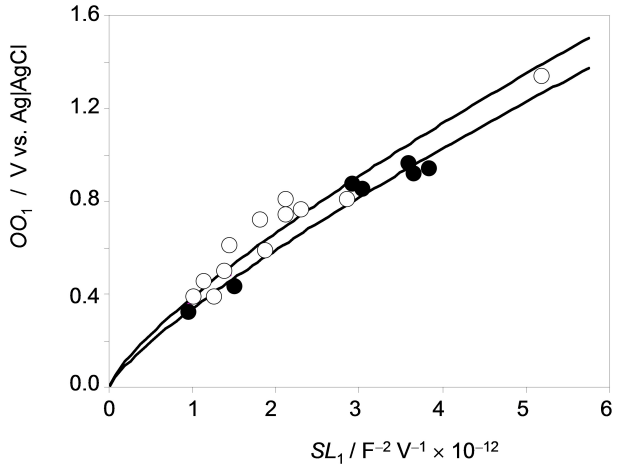

Figure 8. Variation of the OO_1 on SL_1 of the M–S plots corresponding to binary Cu–Sn bronze (solid circles) and copper (circles) samples dating to the Urnfield Culture (1200–900 BCE) and stored in the museums of Graz (Johanneum) and Bad Aussee. The continuous lines correspond to the fit of experimental data to a potential function. From impedance measurements such as shown in Figure 4.

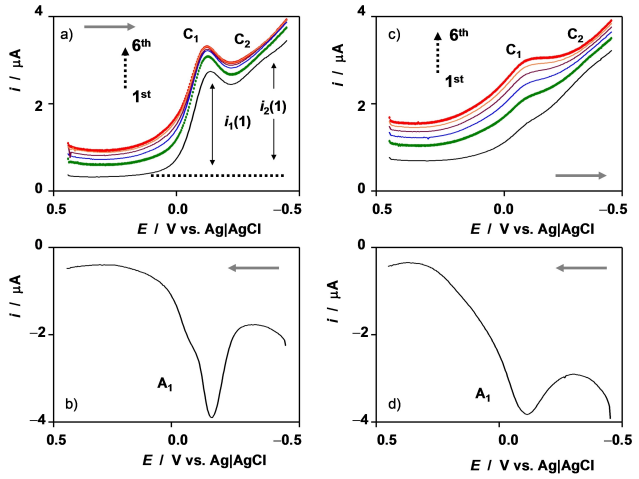

Figure 9. Square wave voltammograms of graphite electrodes modified with samples a,b) AU06 and c,d) Graz02 in contact with air–saturated 0.25 M HAc/NaAc aqueous buffer at pH 4.75. Potential scan initiated at a,c) 0.45 V in the negative direction; b,d) −0.45 V in the positive direction; potential step increment 4 mV; square wave amplitude 25 mV; frequency 10 Hz. Six consecutive scans (dotted arrows) are superimposed in a) and c). The solid arrows indicate the direction of the potential scan.

These results are consistent with VIMP data for the same sample sets. Similar to previously reported studies on archaeological copper, brass, and bronze artifacts,[20–23,29–31] square wave voltammograms of sample–modified graphite electrodes in contact with aqueous acetate buffer show the signals corresponding to the reduction of cuprite and tenorite. Typical voltammograms are shown in Figure 9 for samples AU06 (a casting cake sample from Obertraun-Traunweg, cat. no. 36) and Graz02 (a bronze axe from Buchkogel/Wildon dating to the Late Bronze Age (1200–900 BCE)).

When scanning the potential in the negative direction, a cathodic peak is recorded at ca. −0.15 V vs. Ag/AgCl (C_1). This corresponds to the reduction of cuprite to copper metal and is followed by a more or less intense shoulder at ca. −0.36 V (C_2) representing the reduction of tenorite to copper. The corresponding peak currents ($i_1(N)$, $i_2(N)$) were measured at the N^{th} scan using the criterion shown in Figure 9a. When scanning the potential in the positive direction, a prominent anodic peak at ca. 0.0 V (A_1) marks the oxidation of the previously formed metallic copper deposit to Cu(II) ions in the solution phase. As previously described,[27-29] successive negative-going voltammograms provide information on progressively deeper regions of the corrosion patina of the objects studied using the accumulated peak currents recorded for the processes C_1 and C_2 in successive scans, $I_1(N)$, $I_2(N)$ ($I_J(N) = i_J(1) + i_J(2) + \ldots + i_J(N)$). As in the case of the M–S representations in Figures 5–7, the values of $I_2(6)$ and $I_1(6)$ allow a distinction to be made between the copper and bronze samples of the Late Bronze Age (Urnfield Culture, 1200–900 BCE) from the museums of Graz (Johanneum) and Bad Aussee. As can be seen in Figure 10, despite the relatively large scatter, the data points for the bronze and copper samples can be grouped around two distinct trend lines.

These VIMP results are consistent with the M–S analysis in Figures 6–8 based on OO_1 vs. SL_1 plots. A second sample grouping criterion based on M–S plots is shown in Figure 11. Here, OO_2 vs. OO_1 plots are depicted for samples of a) brass statues from the Hofkirche in Innsbruck, b) brass plaques (Tyrolean State Museums) and bronze samples from the Graz

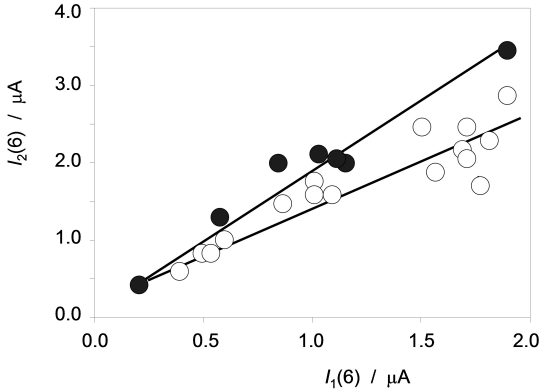

Figure 10. Variation of $I_2(6)$ on $I_1(6)$ for binary Cu–Sn bronze (solid circles) and copper (circles) samples of the Urnfield Culture in the museums of Graz and Bad Aussee. From voltammograms such as depicted in Figure 7a,c. The continuous lines correspond to the linear fit of the experimental data.

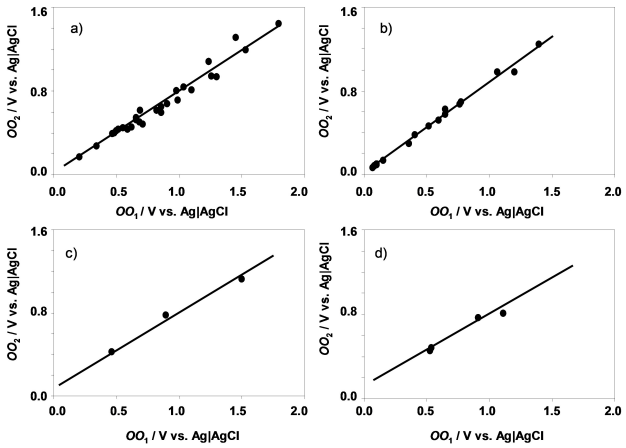

Figure 11. Plots of OO_2 vs. OO_1 determined in Mott–Schottky plots for: a) Samples from the Renaissance statues from Hofkirche in Innsbruck; b) Tyrolean State Museums brass objects; c) Johanneum (Graz) bronze samples of ca. 4000 years old; d) Johanneum (Graz) bronze samples of ca. 6000 years old. The continuous lines correspond to the linear fit of the experimental data. From impedance measurements under conditions as in Figure 4.

Museum of c) ca. 4000 years old and d) 6000 years old. In all cases, the data points define straight lines from the origin but with different slopes. Brass samples from the Hofkirche statuary, all around 500 years old, define a straight line with a slope of 0.80 ± 0.03. This slope coincides with that of brass plaques from the Tyrolean State Museums (0.80 ± 0.03) distributed over a wide period (15th and 17th centuries CE). In the case of approximately 4000-year-old bronze samples in the Graz Museum, the slope is 0.67 ± 0.03 while the equivalent 6000-year-old samples have a slope of 0.64 ± 0.03, thus suggesting the possibility of an age dependence of the variation of OO_2 on OO_1. This hypothesis is consistent with data for bronze samples of the Urnfield Culture (dated back between 1200 and 900 BCE) from the Graz Museum shown in Figure 12. Here, the plot of E_{FB2}^{app} vs. E_{FB2}^{app} can be fitted to a straight trend line with a higher slope (0.78 ± 0.03). These data suggest that the slope of the linear variation of E_{FB2}^{app} on E_{FB2}^{app} could be an age marker whose value decreases with age.

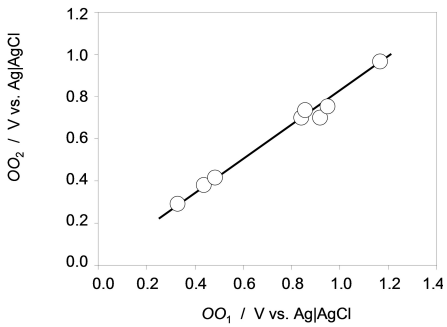

Figure 12. Plots of OO_2 vs. OO_1 determined in Mott–Schottky plots for bronze samples of the Urn Culture from the Johanneum (Graz) Museum. The continuous lines correspond to the linear fit of experimental data. From impedance measurements under conditions as in Figure 4.

All these data support the idea that M–S plots of impedance data can be used as a source of archaeometric information. This technique is of particular interest because of: i) the requirement for nanogram amounts of sample, i.e., at the sub–micro and nano–levels, and ii) by the fact that, by avoiding the application of potentials where faradaic processes occur, repeated analyses can be carried out successively on the same sample.

Conclusions

The application of impedance measurements to sub–micro samples of the corrosion patina of copper–based archaeological objects, abrasively attached to graphite electrodes in contact with 0.10 M Na_2SO_4 aqueous solution yields well–defined Mott–Schottky plots. Consistent with the *p*-type semiconducting nature of the dominant copper corrosion products, cuprite, and tenorite, these plots can be approximated to two linear branches with negative slopes. A simple theoretical model allows these features to be rationalized as resulting from the contribution of the fraction of the graphite electrode directly exposed to the electrolyte solution.

The values of the Mott–Schottky slopes and apparent flat band potentials obtained from the above plots allow the archaeological samples to be grouped. This grouping can be taken as representative of differences in the "gross" composition (mainly copper, bronze, and brass), and/or manufacturing method, and/or age. This grouping is consistent with that obtained from voltammetric data on the same samples in contact with aqueous acetate buffer. Accordingly, Mott–Schottky plots from impedance data can be seen as a new, minimally invasive, analytical tool that complements the existing techniques of archaeometric analysis.

Experimental

Samples were taken from various archaeological and historical objects from museums in Bad Aussee (Kammerhofmuseum), Graz (Johanneum), the Tyrolean State Museums (Hall deposit), and the Renaissance statues from the Hofkirche in Innsbruck (Austria). The list of objects (124 in total) and their characteristics is given in Supplementary Information, Tables S.1 to S.8. These include 28 statues from the Hofkirche/Innsbruck (24 brass and 4 copper statues), 47 brass, bronze, and Ag–Cu and Au–Cu objects from the deposit in Hall of the Tyrolean State Museums, 26 objects from the Johanneum Graz, 23 objects (mainly, copper casting cake) from the Kammerhofmuseum in Bad Aussee, 26 objects from Archaeological Heritage Office in Genoa (soprintendenza), and 14 objects from the museo civico in San Remo. The examined samples cover a time interval between the Bronze Age and the 18th century. Depending on the size of the objects 1–3 samples were taken from each object. Complementary experiments were carried out on Eurocent coins with brown patina.

Sampling was performed by pressing a graphite bar (Faber-Castell HB type, diameter 2 mm) over the surface of the object. The graphite rod was previously polished on paper as is common in VIMP.[24,25] Sampling (2–3 samples per artifact) was carried out on flat areas of the objects with a uniform brownish or blackish color.

The samples were taken in the museums under the supervision of the technical staff.

Impedance and voltammetric measurements were carried out at the Department of Analytical Chemistry of the University of Valencia (Spain) using a CH I920c potentiostat (Cambria Scientific, Llwynhendy, Llanelli UK). A conventional three-electrode configuration was used at room temperature ($25 \pm 1\,^{\circ}C$). The 25 mL cell contained the sample-modified graphite rod as the working electrode, a platinum wire auxiliary electrode and an Ag/AgCl (3 M NaCl) reference electrode. To obtain M–S data, impedance measurements were carried out using the experimental conditions reported by Jeong et al.[31] for the study of Cu_2O/CuO nanostructured architectures: electrolyte 0.10 M Na_2SO_4 (pH 6.28) aqueous solution and potentials between 0.0 and 1.0 V vs. Ag/AgCl. Frequencies between 10^2 and 10^5 Hz were used. EIS experiments were performed under the same conditions in the 0.1 to 10^5 Hz frequency range with ac sinusoidal perturbation (peak-to-peak) amplitude of 10 mV at the open circuit potential (OCP) determined during equilibration for 5 min. The same electrode configuration was used for the VIMP measurements, with an optional deaerated 0.25 M HAc/NaAc solution (Probus Reagents) at pH 4.75 as the supporting electrolyte.

Supporting Information

List of studied objects containing relevant archaeological an compositional data; additional voltametric records and data processing.

Acknowledgements

Project P34960-G supported by the Austrian Science Fund (FWF), project PID2020-113022GBI00 supported by MCIN/AEI/10.13039/501100011033, Fondo Europeo de Desarrollo Regional (ERDF) and Agencia Estatal de Investigación (AEI), and Project AICO/2021/095 which is supported with Generalitat Valenciana and Fondo Europeo de Desarrollo Regional (ERDF), funds are gratefully acknowledged. Dr. Manuel Gozalbes and Museu de Prehistòria de València are also gratefully acknowledged.

Conflict of Interests

The authors declare no conflict of interest.

Data Availability Statement

The data that support the findings of this study are available from the corresponding author upon reasonable request.

Keywords: Archaeometry · Brass · Bronze · Copper · Mott–Schottky

[1] B. W. Roberts, C. Thornton, Eds. *Archaeometallurgy in Global Perspective. Methods and Syntheses* Springer, Berlin, **2014**.
[2] M. F. Alberghina, R. Barraco, M. Brai, T. Schillaci, L. Tranchina, *Spectrochim. Acta B* **2011**, *66*, 129.
[3] P. Letardi, B. Salvadori, M. Galeotti, A. Cagnini, S. Porcinai, A. Santagostino Barbone, A. Sansonetti, *Microchem. J.* **2016**, *125*, 151.
[4] A. Inberg, D. Ashkenazi, M. Cohen, N. Iddan, D. Cvikel, *Microchem. J.* **2018**, *143*, 400.
[5] M. T. Doménech-Carbó, C. Álvarez-Romero, A. Doménech-Carbó, L. Osete-Cortina, M. L. Martínez-Bazán, *Microchem. J.* **2019**, *148*, 573.
[6] D. A. Scott, *J. Am. Ite. Cons.* **1994**, *33*, 1.
[7] L. Robbiola, J. M. Blengino, C. Fiaud, *Corros. Sci.* **1998**, *40*, 2083.
[8] I. Constantinides, A. Adriaens, F. Adams, *Appl. Surf. Sci.* **2002**, *189*, 90.
[9] L. Robbiola, R. Portier, *J. Cult. Herit.* **2006**, *7*, 1.
[10] C. Chiavari, K. Rahmouni, H. Takenouti, S. Joiret, P. Vermaut, L. Robbiola, *Electrochim. Acta* **2007**, *52*, 7760.
[11] M. C. Bernard, S. Joiret, *Electrochim. Acta* **2009**, *54*, 5199.
[12] G. Bertrand, E. Rocca, C. Savall, C. Rapin, J. .-C. Labrune, P. Steinmetz, *J. Electroanal. Chem.* **2000**, *489*, 38.
[13] A. Xu, C. Dong, X. Wei, X. Li, D. D. Macdonald, *J. Electroanal. Chem.* **2019**, *834*, 216.
[14] E. Cano, A. Crespo, D. Lafuente, B. Ramírez Barat, *Electrochem. Commun.* **2014**, *41*, 16.
[15] B. Ramírez Barat, E. Cano, *ChemElectroChem* **2019**, *6*, 2553.
[16] A. Sassolini, N. Colozza, E. Papa, K. Hermansson, I. Cacciotti, F. Arduini, *Electrochem. Commun.* **2019**, *98*, 69.
[17] A. Doménech-Carbó, M. A. Peiró-Ronda, J. Vives-Ferrándiz, G. S. Duffó, S. Farina, *Electrochem. Commun.* **2021**, *125*, 106992.
[18] A. Doménech-Carbó, M. T. Doménech-Carbó, C. Álvarez-Romero, N. Montoya, T. Pasíes-Oviedo, M. Buendía-Ortuño, *Electroanalysis* **2017**, *29*, 2008.
[19] A. Doménech-Carbó, M. T. Doménech-Carbó, C. Álvarez-Romero, T. Pasíes-Oviedo, M. Buendía-Ortuño, *Electroanalysis* **2019**, *31*, 1164.
[20] M. Di Fazio, A. C. Felici, F. Catalli, M. T. Doménech-Carbó, C. De Vito, A. Doménech-Carbó, *Microchem. J.* **2020**, *152*, 104306.
[21] A. Doménech-Carbó, M. T. Doménech-Carbó, E. Montagna, C. Álvarez-Romero, Y. Lee, *Talanta* **2017**, *169*, 50.
[22] N. Montoya, E. Montagna, Y. Lee, M. T. Doménech-Carbó, A. Doménech-Carbó, *J. Raman Spectrosc.* **2017**, *48*, 1337.
[23] F. Scholz, U. Schröder, R. Gulabowski, A. Doménech-Carbó, *Electrochemistry of Immobilized Particles and Droplets* 2nd ed. Springer, Berlin-Heidelberg, **2014**, p. 94.
[24] A. Doménech-Carbó, J. Labuda, F. Scholz, *Pure Appl. Chem.* **2013**, *85*, 609.
[25] A. Doménech-Carbó, M. T. Doménech-Carbó, *Pure Appl. Chem.* **2018**, *90*, 447.
[26] A. Doménech-Carbó, M. T. Doménech-Carbó, *Electrochemistry for Cultural Heritage, Monographs in Electrochemistry series* F. Scholz, L. Péter Eds. Berlin-Heidelberg, **2023**, pp. 272–289.
[27] A. Doménech-Carbó, M. Donnici, C. Álvarez-Romero, S. Daniele, M. T. Doménech-Carbó, *J. Solid State Electrochem.* **2021**, *25*, 195.
[28] A. Doménech-Carbó, M. Mödlinger, M. T. Doménech-Carbó, *J. Electroanal. Chem.* **2021**, *893*, 115336.
[29] A. Doménech-Carbó, M. Mödlinger, L. Osete-Cortina, M. T. Doménech-Carbó, *ChemElectroChem.* DOI: 10.1002/celc.202300405.
[30] N. A. M. Shanid, M. A. Kadar, *Thin Solid Films* **2008**, *516*, 6245.
[31] D. Jeong, W. Jo, J. Jeong, T. Kim, S. Han, M. .-K. Son, H. Jung, *RSC Adv.* **2022**, *12*, 2632.
[32] M. Mödlinger, P. Trebsche, *Archaeol. Anthropol. Sci.* **2021**, *13*, 125.
[33] M. Mödlinger, *Herstellung und Verwendung bronzezeitlicher Schwerter Mitteleuropas. Eine vertiefende Studie zur mittelbronze- und urnenfelderzeitlichen Bewaffnung und Sozialstruktur. Universitätsforschungen zur prähistorischen Archäologie* **2021**, Habelt Verlag, Bonn, pp. 137–148.
[34] M. Mödlinger, *Protecting the body in war and combat: metal body armour in Bronze Age Europe, Oriental and European Archaeology 6.* ÖAW, Vienna, **2017**, pp. 149–157, 202–204, and 255–256.
[35] M. Mödlinger, P. Trebsche, B. Sabatini, *PLoS One* **2021**, *16*, e0254096.
[36] M. Mödlinger, B. Asmus, G. Ghiara, *Int. J. Metalcast.* **2024** (in press). DOI: 10.1007/s40962-024-01299-4
[37] A. Hankin, F. E. Bedoya-Lora, J. C. Alexander, A. Regoutz, G. H. Kelsall, *J. Mater. Chem.* A **2019**, *7*, 26162.
[38] A. Doménech-Carbó, *Electrochemistry of Porous Materials* 2nd Ed. Taylor & Francis, Boca Raton, **2021**, pp. 124-126.
[39] T. Kida, G. Guan, Y. Minami, T. Ma, A. Yoshida, *J. Mater. Chem.* **2003**, *13*, 1186.

[40] A. van Dijken, E. A. Meulenkamp, D. Vanmaekelbergh, A. Meijerink, *J. Lumin.* **2000**, *90*, 123.
[41] N. N. Syrbu, I. M. Tiginyanu, V. V. Zalamai, V. V. Ursaki, E. V. Rusu, *Physica B+C* **2004**, *353*, 111.
[42] M. V. Makarova, K. Macounová, P. J. Krtil, *J. Solid State Electrochem.* **2006**, *10*, 320.
[43] A. Adán-Mas, T. M. Silva, L. Guerlou-Demourgues, M. F. Montemor, *Electrochim. Acta* **2018**, *289*, 47.
[44] K. F. Young, H. K. R. Frederikse, *J. Phys. Chem. Ref. Data* **1973**, *2*, 313.
[45] A. A. Meza, U. C. Irvine, ProQuest ID: Meza_uci_0030D_18309, **2023**, Merritt ID: ark:/13030/m5sz74vp.
[46] P. Yi, C. Dong, K. Xiao, C. Man, X. Li, *J. Electroanal. Chem.* **2018**, *809*, 52.
[47] N. A. Mohemmed Shanid, M. Abdul Khadar, *Thin Solid Films* **2008**, *516*, 6245.
[48] L. Robbiola, K. Rahmouni, C. Chiavari, C. Martini, D. Prandstaller, A. Texier, H. Takenouti, P. Vermaut, *Appl. Phys. A* **2008**, *92*, 161.
[49] V. Oberhammer, *Die Bronzestandbilder des Maximiliangrabmales in der Hofkirche zu Innsbruck*. Tyrolia Verlag, Innsbruck, **1935**.
[50] K. Oettinger, *Die Bildhauer Maximilians am Innsbrucker Kaisergrabmal*. Hans Carl, Nürnberg, 1966.
[51] R. Krause, *Studien zur kupfer- und frühbronzezeitlichen Metallurgie zwischen Karpatenbecken und Ostsee* Rahden/Westf. **2003**.
[52] J. M. Del Hoyo-Meléndez, M. Matosz, A. Walanus, P. Krupska-Wolas, *Microchem. J.* **2023**, *51*, 104156.

Manuscript received: November 7, 2023
Revised manuscript received: January 29, 2024
Version of record online: March 20, 2024